



**HAL**  
open science

**Post-orogenic extension and metamorphic core complexes in a heterogeneous crust: the role of crustal layering inherited from collision. Application to the Cyclades (Aegean domain)**

Benjamin Huet, Laetitia Le Pourhiet, Loic Labrousse, Evgenii E.B. Burov,  
Laurent Jolivet

► **To cite this version:**

Benjamin Huet, Laetitia Le Pourhiet, Loic Labrousse, Evgenii E.B. Burov, Laurent Jolivet. Post-orogenic extension and metamorphic core complexes in a heterogeneous crust: the role of crustal layering inherited from collision. Application to the Cyclades (Aegean domain). *Geophysical Journal International*, 2011, 184, pp.611-625. 10.1111/j.1365-246X.2010.04849.x . insu-00564011

**HAL Id: insu-00564011**

**<https://insu.hal.science/insu-00564011>**

Submitted on 5 Feb 2013

**HAL** is a multi-disciplinary open access archive for the deposit and dissemination of scientific research documents, whether they are published or not. The documents may come from teaching and research institutions in France or abroad, or from public or private research centers.

L'archive ouverte pluridisciplinaire **HAL**, est destinée au dépôt et à la diffusion de documents scientifiques de niveau recherche, publiés ou non, émanant des établissements d'enseignement et de recherche français ou étrangers, des laboratoires publics ou privés.

# Post-orogenic extension and metamorphic core complexes in a heterogeneous crust: the role of crustal layering inherited from collision. Application to the Cyclades (Aegean domain)

Benjamin Huet,<sup>1,2</sup> Laetitia Le Pourhiet,<sup>1,2</sup> Loic Labrousse,<sup>1,2</sup> Evgenii Burov<sup>1,2</sup> and Laurent Jolivet<sup>3</sup>

<sup>1</sup>UPMC Univ Paris 06, UMR 7193, ITeP, F-75005, Paris, France. E-mail: benjamin.huet@upmc.fr

<sup>2</sup>CNRS, UMR 7193, ITeP, F-75005, Paris, France

<sup>3</sup>ISTO, UMR 6113, Université d'Orléans 1A, Rue de la Férollerie, 45071 Orléans Cedex 2, France

Accepted 2010 October 14. Received 2010 September 22; in original form 2010 February 19

## SUMMARY

The development of metamorphic core complexes (MCC) corresponds to a mode of lithospheric continental stretching that follows collision. In most of the models that explain the formation of the MCC, high thermal gradients are necessary to weaken the lower crust and to induce its ascent. Such models fail to explain the exhumation of high pressure–low temperature metamorphic rocks in metamorphic core complex structures as observed in the Cycladic Blueschists in the Aegean domain. Besides, account for the lithological crustal stratification induced from collision has never been tested. In this paper, we use fully coupled thermomechanical modelling to investigate the impact of structural heritage and initial thermal gradient on the behaviour of the post-orogenic continental lithosphere. The models are designed and validated by petrological, structural and time data from the Cyclades. As a result, high thermal gradients (Moho temperature higher than 800°C) are neither necessary nor always sufficient to induce the development of a metamorphic core complex. At the contrary, the rheological layering of the crust inherited from collision is a first-order parameter controlling the development of extensional structures in post-orogenic settings. ‘Cold’ MCC can develop if the crust is made of a strong nappe thrust on top of weaker metamorphic cover and basement units, as observed in the Cyclades.

**Key words:** Back-arc basin processes; Continental tectonics: compressional; Continental tectonics: extensional; Dynamics of lithosphere and mantle; Crustal structure; Rheology: crust and lithosphere.

## 1 INTRODUCTION

### 1.1 Metamorphic core complexes: characteristic features

Metamorphic core complexes (MCC) are crustal-scale structures that exhibit ductilely deformed high-grade rocks exhumed below a low-angle normal-fault or detachment. Since their identification in the Basin and Range (Coney 1980), such structures have been extensively studied through field work, geophysical imaging and modelling. From extensive field studies [for general review see (Whitney *et al.* 2004)] the main characters of MCC can be outlined as follows: (1) a characteristic size of some tens of kilometres sometimes reaching a hundred kilometres, (2) a dome core, made of metamorphic rocks, migmatites and granite bounded, (3) a detachment zone and (4) upper-crustal units with limited metamorphism and detrital sedimentary basins.

The regions where these structures were described all represent former orogens. It is now widely accepted that MCC and their detachments are characteristic features of post-orogenic extension in initially thickened continental crust where Moho temperatures may be higher than 700°C (Gaudemer *et al.* 1988). Assuming a granitic crustal composition, the lower crust behaves as a weak ductile layer able to flow horizontally at significant regional scale (Block & Royden 1990; Buck 1991), which is consistent with the occurrence of migmatitic cores (Rey *et al.* 2009). The conceptual model of ‘fluid crustal layer’ (Wernicke 1990) constitutes the basis of most older simplified numerical and experimental models of MCC (e.g. Wdowinski & Axen 1992; Lavier *et al.* 1999; Chéry 2001). Recent MCC models which account for temperature-dependent viscous rheology in lower crust and mantle suggest that MCC development can be only reproduced for initial Moho temperatures higher than 800°C and for minimal crustal thicknesses of 45 km (Tirel *et al.*

2008). The MCC are therefore considered to be restricted to warm crusts.

## 1.2 Role of the initial geometry of the thickened crust

While recovering some of the first-order characteristics of most of the MCC, the previous models failed at explaining the limited retrograde heating within some exhumed high pressure–low temperature (HP–LT) metamorphic units, as is observed in the Cycladic MCC (Okrusch & Broecker 1990). On Tinos in the northern part of Cyclades, the pressure–temperature–time ( $P$ – $T$ – $t$ ) data suggest temperatures as cold as 680°C–700°C (Parra *et al.* 2002) at 50 km depth at the beginning of crustal extension, well below the 800°C lower bound established for the initial Moho temperature (Tirel *et al.* 2008).

Most of the models implicitly consider that thickening of the crust is coaxial and homogeneous leading to a thick ‘normal’ stratification. The geological reality is, however, that most orogens formed as a result of nappe stacking. Consequently, it is possible to assume that the structure of a crustal orogenic wedge is different from the ‘normal’ sequence, with stronger mafic allochthons thrust on top of a weaker autochthon. Such an orogenic sequence must have mechanical properties remarkably differing from those of normal crust. Specifically nappe stacking may result in strong mechanical properties remarkably differing from those of normal crust. After a brief review of the available data concerning the Cyclades, taken as a reference for ‘cold MCC’, and a presentation of chosen numerical model setups, the experiments will be interpreted and validated by comparing predicted structure and synthetic  $P$ – $T$  paths to natural data in the Cyclades.

In this paper, we investigate through thermomechanical modelling how a crustal stratification inherited from nappe stacking may affect the development of MCC during post-orogenic extension. We focus on the relative influence of initial stratification and thermal gradient of the crust on the behaviour of continental lithosphere during post-orogenic extension. After a brief review of the available data concerning the Cyclades, taken as a reference for ‘cold MCC’, and a presentation of chosen numerical model setups, the experiments will be interpreted and validated by comparing predicted structure and synthetic  $P$ – $T$  paths to natural data in the Cyclades.

## 2 EVIDENCE FOR INHERITED CRUSTAL STRATIFICATION IN THE CYCLADIC MCC

### 2.1 Geological setting

The Cycladic islands, in the Aegean sea (Fig. 1A), belong to the internal part of the Hellenide–Tauride belt (Jacobshagen *et al.* 1978). Two trends of MCC are distinguished: in the northern Cyclades, the MCC of Andros, Tinos, Mykonos and Ikaria were exhumed below a series of northeast dipping detachments (Jolivet *et al.* 2010), while the MCC of Paros and Naxos, in the central Cyclades, lie below the north-dipping central Cycladic Detachment (Gautier *et al.* 1993; Vanderhaeghe 2004). Both sets of detachments are associated to top-to-the-north or northeast shearing ductile deformation in the lower plate. HT–LP metamorphism in amphibolite and greenschist facies conditions accompanied the exhumation of the lower plate. This tectono-metamorphic event has been linked to the extension of the Aegean lithosphere in the backarc domain of the Hellenic subduction zone, triggered by the southward retreat of the African slab (Le Pichon & Angelier 1981; Jolivet & Faccenna 2000). The formation of these MCC is considered as coeval with backarc mag-

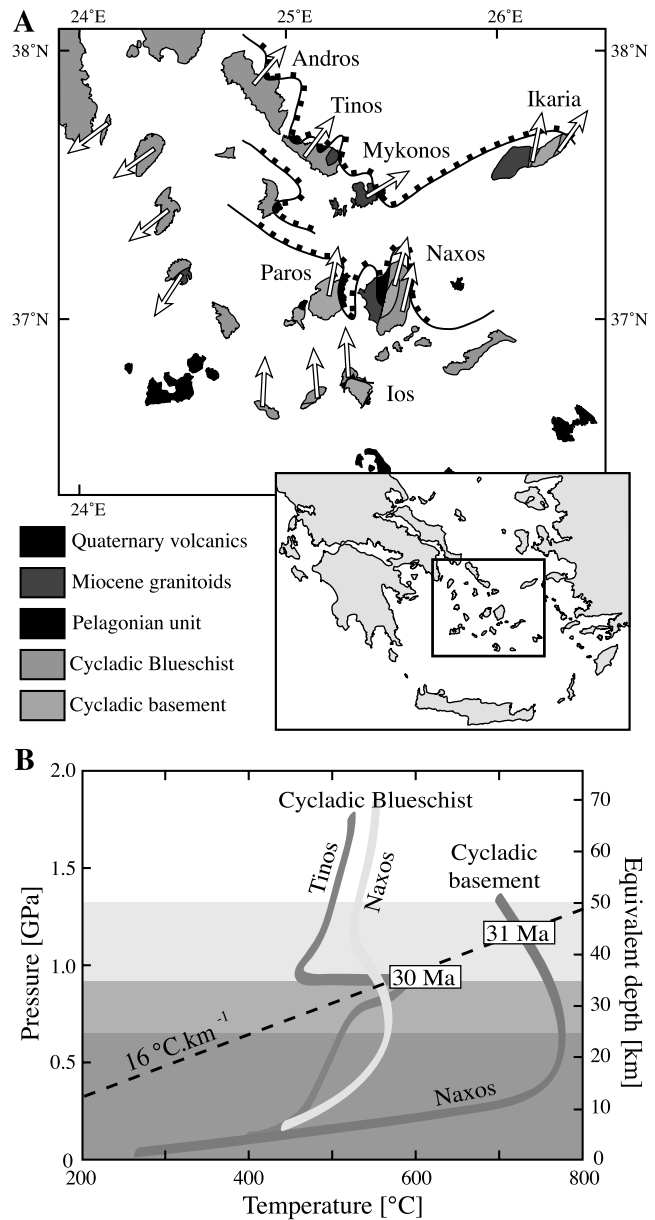


**Figure 1.** (A) Structural map of the Cyclades (Huet *et al.* 2009). The MCC are associated to north-dipping detachments and to top-to-the-north or north-east deformation in the lower plate (Cycladic Blueschist and Cycladic basement). The Pelagonian unit constitutes the upper plate of the MCC. The white arrows indicate the sense of ductile shear in the lower plate. (B)  $P$ – $T$ – $t$  paths of the Cycladic Blueschist of Tinos (Parra *et al.* 2002), the Cycladic Blueschist and the Cycladic basement of Naxos (Martin 2004). The equivalent depth is computed assuming lithostatic pressure and a density of 2700 kg m<sup>-3</sup>. The pressure of the two units recorded at 30 Ma defines an initial thermal gradient of 16°C km<sup>-1</sup>. The inferred stratification of the crust before the onset of extension is represented by the grey background (dark grey: upper crust, median grey: middle crust and light grey: lower crust).

matism that initiated at 35–30 Ma and migrated southwards with slab retreat at 1 cm yr<sup>-1</sup> (Jolivet & Brun 2009).

Between 30 and 10 Ma, three crustal units have been involved in the formation of the MCC; they belong to the Hellenides nappe stack formed during the Eocene (Bonneau 1984). The lower Cycladic basement unit crops out in the central and southern Cyclades (Fig. 1A). The middle Cycladic Blueschist unit is present on most

islands. Both units form the lower plate of the MCC. They exhibit HP–LT Eocene metamorphic parageneses with variable degree of preservation, reworked in higher temperature conditions during the Oligo-Miocene (Altherr *et al.* 1982; Wijbrans & McDougall 1986). The Pelagonian unit appears in the hangingwall of the detachments. The initial thickness of the crust and individual nappes before the onset of extension is poorly constrained. A value of 50 km has been proposed (McKenzie 1978) and is now often adopted. We use the following thicknesses for the three units: 20 km for the Cycladic basement in lower crust position, 10 km for the Cycladic Blueschist unit in middle crust position and 25 km for the Pelagonian unit in upper crust position (Fig. 1B). These values are consistent with the pressure recorded in the two lower units at 30 Ma (Parra *et al.* 2002; Martin 2004), assuming that pressure is close to lithostatic and that the crustal density is  $2700 \text{ kg m}^{-3}$  (Fig. 1B).

## 2.2 Deformation pattern in the Cycladic MCC units

The Cycladic Basement is mainly composed of hercynian granitoids and gneiss overlain by a thin layer of micaschists. The lowermost part of this unit is exposed on Naxos and Paros where pervasive partial melting is observed (Jansen & Schuiling 1976). The uppermost part of this unit crops out on Ios where it is free of Cenozoic migmatization. On this island, large low-strain zones of granite are bounded by narrow shear zones (Vandenberg & Lister 1996; Huet *et al.* 2009). A strain gradient can be observed from the preserved core of the unit to its upper contact with the Cycladic Blueschist. The Cycladic Blueschist is an association of metapelite, marble and metabasite. Extensional deformation evolved during exhumation from distributed shear to pervasive ductile shear-bands and finally to localized shallow-dipping normal faults (Mehl *et al.* 2005). This unit also exhibits a strain gradient from bottom to top, associated to a gradient of retrogression of the HP–LT parageneses (Parra *et al.* 2002). The Pelagonian unit is composed of ophiolitic material and slivers of gneissic continental crust. In this unit, extension has essentially been accommodated by normal faulting (Katzir *et al.* 1996), with only minor ductile deformation at its base. Consequently, during the first stages of the exhumation in the MCC, the brittle–ductile transition (BDT) in the crust corresponded more or less to the Pelagonian/Cycladic Blueschist contact. Moreover, the reactivation of nappe contacts evidences that strain localization is mainly due to the rheological contrasts between units. Hence, lithology seems to control the mechanical behaviour of the crust during the formation of the Cycladic MCC, except when migmatization occurs.

## 3 DESIGN OF THE NUMERICAL EXPERIMENTS

### 3.1 The numerical code

The numerical code FLAMAR v12 used in this study is based on the FLAC algorithm (Cundall 1989) and is a result of long evolution of Paravoz v3 (Poliakov *et al.* 1993) and its later versions (Toussaint *et al.* 2004; Yamato *et al.* 2007). It solves simultaneously for conservation of momentum

$$\rho g_i + \frac{\partial \sigma_{ij}}{\partial x_j} = \rho \frac{\partial V_i}{\partial t}, \quad (1)$$

and for conservation of heat

$$\frac{DT}{Dt} = \frac{\partial T}{\partial x_i} \left( \chi \frac{\partial T}{\partial x_i} \right) + H_r. \quad (2)$$

The parameters  $\rho$ ,  $g$ ,  $\sigma$ ,  $x$ ,  $V$ ,  $t$ ,  $T$  and  $\chi$  stand, respectively, for density, gravity acceleration, stress, coordinate, velocity, time, temperature and thermal diffusivity. In all cases of this study, we switched off the internal heating term,  $H_r$ , due to uncertainties on its values in case of nappe stacking (*cf.* Section 7.1). Thermomechanical coupling is enforced using Boussinesq approximation for the computation of density, including thermal stresses in eq. (1) and advecting the temperature with the mesh within the Lagrangian formulation of the code. The rock behaviour is approximated by explicit visco-elasto-plastic rheology (power-law ductile-viscous flow law and Mohr–Coulomb plasticity). The effective rheological behaviour is determined by current strain-rate, state of stress and temperature [the implementation is detailed in Le Pourhiet *et al.* (2004)]. A robust marker-based remeshing procedure allows for handling of very large strains and displacements (Yamato *et al.* 2007). To focus on the influence of the rheological stratification, the model setups are deliberately simplified. Erosion, shear-heating, partial melting and mineral phase transitions are not considered in the computation. A passive marker technique (Yamato *et al.* 2007) allows for tracing synthetic  $P$ – $T$  paths and computing synthetic finite deformation field, that is, schistosity and intensity of finite strain.

### 3.2 Initial and boundary conditions

The thermal boundary conditions (Fig. 2) are set as follows:  $0^\circ\text{C}$  at the surface, fixed initial temperature at the bottom (1100, 1300 or  $1500^\circ\text{C}$ ) and zero lateral outflow at the sides of the model. The three thermal profiles are initially in equilibrium with the boundary conditions (Fig. 2B). The cold, intermediate and warm cases lead to 13.7, 16.2 and  $18.7^\circ\text{C km}^{-1}$  thermal gradient and 685, 810

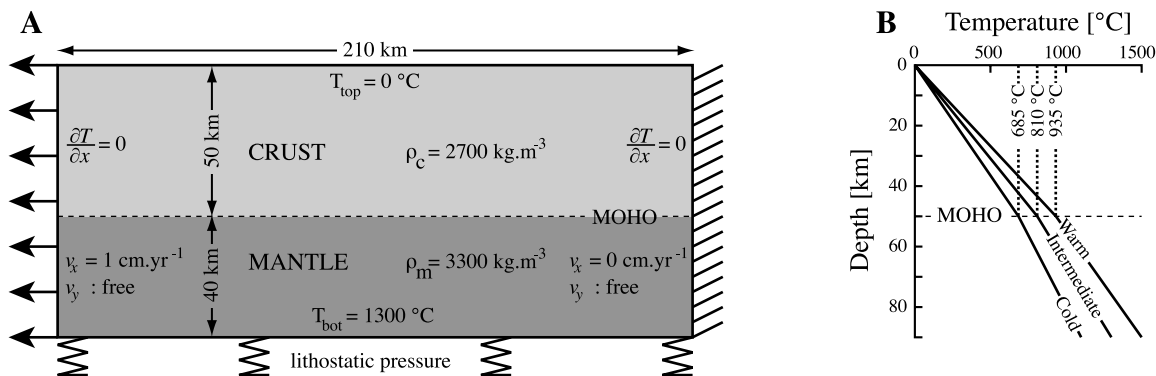


**Figure 2.** (A) Initial and boundary conditions of the experiments. (B) Initial thermal profiles computed for bottom temperatures of 1100, 1300 and  $1500^\circ\text{C}$ .

**Table 1.** Value of physical parameters used in experiments.  $A$ ,  $n$  and  $\Delta G$  are the parameters for power-law creep:  $d\varepsilon/dt = A \sigma^n \exp(-\Delta G/RT)$ . 1 (Ranalli & Murphy 1987), 2 (Hansen & Carter 1982) and 3 (Chopra & Paterson 1984).

All materials							
Shear modulus (GPa)							30
Poisson's ratio							0.25
Mohr-Coulomb criterion							
Cohesion (MPa)							20
Friction angle (°)							30
Thermal expansion coefficient (K <sup>-1</sup> )							$3 \times 10^{-5}$
Specific heat (J kg <sup>-1</sup> K <sup>-1</sup> )							$10^3$
	Density at 25°C 25°C (kg m <sup>-3</sup> )	Thermal conductivity (W m <sup>-1</sup> K <sup>-1</sup> )	A (MPa <sup>-n</sup> s <sup>-1</sup> )	n	$\Delta G$ (kJ mol <sup>-1</sup> )	Material	Ref.
Crust	2700	2.5	$6.7 \times 10^{-6}$	2.4	156	Dry quartzite	1
			$2 \times 10^{-6}$	3.3	186	Dry granite	2
			$1.3 \times 10^{-3}$	2.4	219	Quartz-diorite	2
Mantle	3300	3.3	$2.5 \times 10^4$	3.5	532	Dry dunite	3

**Table 2.** Lithological layering of the three types of experiments.

		REF	PS	NS
Upper crust	Initial thickness (km)	25	10	25
	Lithology	Quartz-diorite	Dry quartzite	Quartz-diorite
Middle crust	Initial thickness (km)	10	15	10
	Lithology	Quartz-diorite	Dry granite	Dry quartzite
Lower crust	Initial thickness (km)	15	25	15
	Lithology	Quartz-diorite	Quartz-diorite	Dry granite
Lithospheric mantle	Initial thickness (km)	40	40	40
	Lithology	Dry dunite	Dry dunite	Dry dunite

and 935 °C at the Moho, respectively. The gradient of the intermediate case is similar to the one deduced from the  $P$ - $T$ - $t$  paths at 30 Ma (Fig. 1B). Both sides of the models have been assigned a free slip condition. Following Tirel *et al.* (2004a), asymmetric lateral boundary conditions are applied, with constant horizontal velocity of 1 cm yr<sup>-1</sup> and 0 cm yr<sup>-1</sup> applied to the left- and the right-end sides, respectively. The upper surface is free while the base deforms in response to hydrostatic forces ensuring local isostatic compensation [Winkler foundation, e.g. Burov & Poliakov (2001)]. The initial velocity field is linearly interpolated from the boundary conditions and stress is initially lithostatic and isotropic. We did not impose any mechanical or thermal heterogeneity to achieve strain localization in some prescribed zone. Instead, a random noise of 5 MPa has been added to the mean cohesion value (20 MPa) in the upper crust thus mimicking natural variability in rock properties (Huisman *et al.* 2005). However, the cohesion of the 15-km-long zone located on the left side of the model has been set to 30 MPa to prevent undesired strain localization on the faster boundary.

### 3.3 Geometry and lithological stratification

The model (Fig. 2) is initially 210 km wide and 90 km thick (crust: 50 km, lithospheric mantle: 40 km) with  $0.75 \times 1.25$  km quadrilateral elements. Three initial crustal stratifications are considered (Tables 1 and 2). The reference (REF) stratification refers to a homogeneous quartz-dioritic 50 km crust, which is the classical geometry studied in MCC modelling studies (Tirel *et al.* 2004a; Tirel *et al.* 2008; Tirel *et al.* 2009). The pure-shear (PS) stratification refers to a commonly accepted rheological stratification: soft upper crust, intermediate strength middle crust and more mafic and stronger

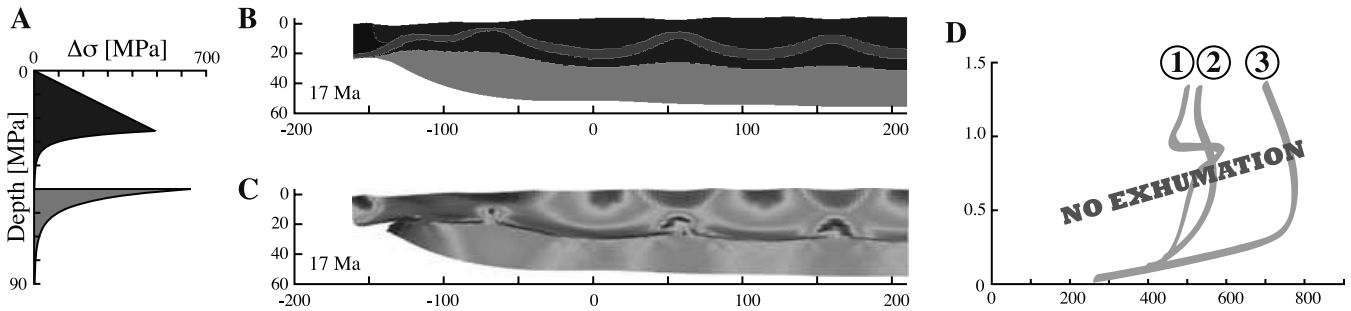
lower crust. The nappe-stacking (NS) stratification refers to an inverted crustal structure and fits the initial geometry inferred for the Cyclades: mafic upper crust, soft middle crust and intermediate strength lower crust. The nine numerical experiments presented here were run for 20 Myr. They correspond to the three rheological stratifications tested for the three given initial thermal profiles (cold, intermediate and warm).

Since the crust is homogeneous in REF experiments, its effective rheology is mainly controlled by temperature (Figs 3A, E and I). In PS and NS experiments, the effective rheology is primarily controlled by the lithological stratification. PS experiments are characterized by two low viscosity layers, a thin one at the base of the middle crust and a thicker one at the base of the lower crust (Figs 4 A, E and I). In both cases, the viscosity decreases continuously with depth. This contrasts with NS experiments, in which a sharp viscosity discontinuity (two orders of magnitude) occurs at the base of the upper crust (Figs 5 A, E and I). Moreover, these experiments are characterized by a thick low viscosity layer that includes both the middle and lower crusts.

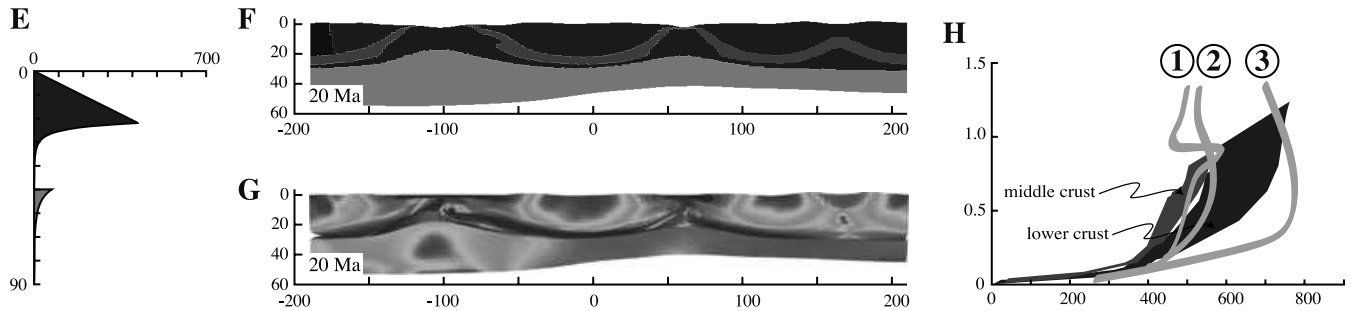
## 4 POST-OROGENIC THERMOMECHANICAL EVOLUTION OF LITHOLOGICALLY LAYERED LITHOSPHERES

All experiments show similar evolutions during the first 2 Myr. Three regularly spaced (70 km) symmetrical grabens form and localize deformation in the upper crust (g1, g2 and g3 on Fig. 6). However, after this initial phase, the rheological profile of the crust controls the localization of strain in deeper layers and results either in a distributed, or in a localized mode of extension in the crust. In

Cold case (initial Moho temperature: 685 °C)



Intermediate case (initial Moho temperature: 810 °C)



Warm case (initial Moho temperature: 935 °C)

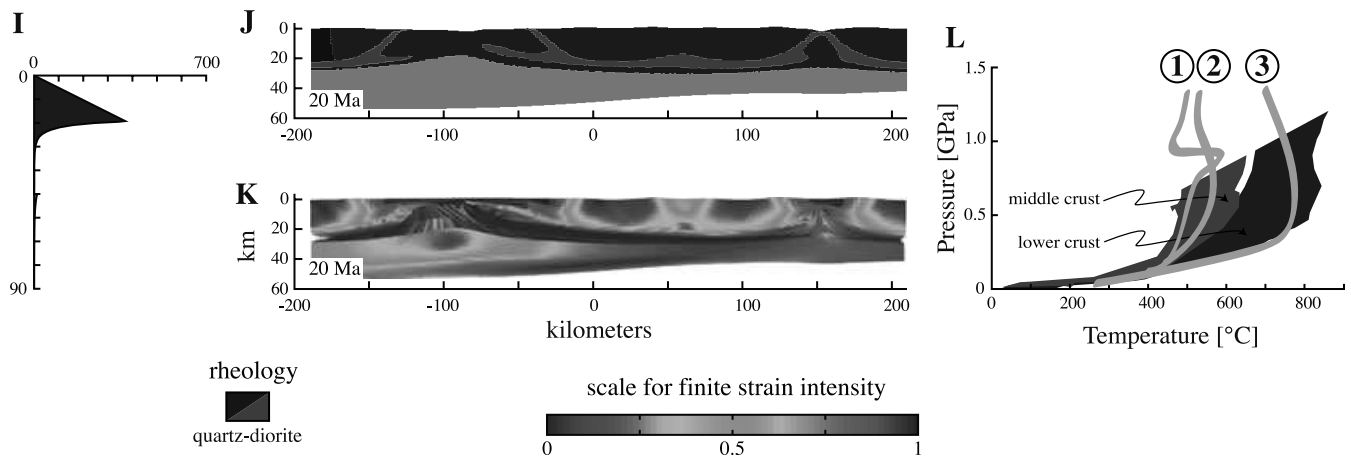


**Figure 3.** Cold, intermediate and warm REF experiments (homogeneous crust). Initial strength profiles (A, E and I), geometry (B, F and J) and intensity of finite strain (C, G and K) at the end of the experiment and comparison between the envelopes of the synthetic  $P$ - $T$  paths and the  $P$ - $T$  paths of Tinos (1) (Parra *et al.* 2002) and Naxos (2 and 3) (Martin 2004) (D, H and L). The black portion of the upper crust in (B, F and J) corresponds to a zone of 30 MPa cohesion introduced to avoid localization at the edge of the model. The mid-crustal layer in (B, F and J) is a passive marker. In the cold case, no middle and lower crust is exhumed at the surface; strength localizes in the mantle leading to the formation of a ‘true rift’. In the intermediate and warm cases, middle and lower crusts are exhumed in ‘spreading dome’ structures. See text for detailed description.

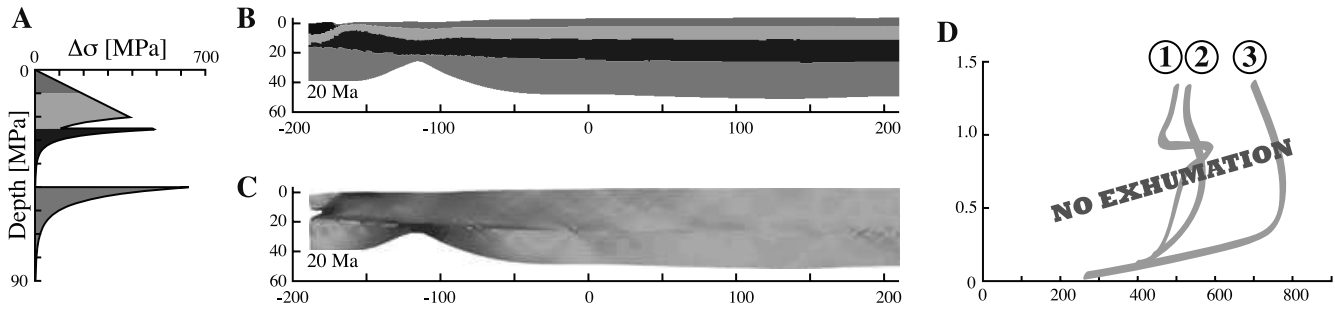
this section we first describe the dynamics of cases with intermediate thermal structure for each tested rheological stratification. We then discuss the effect of the initial thermal profile. Movies showing the evolution of the nine experiments are provided online as Supporting Information.

#### 4.1 The ‘reference’ (REF) experiment

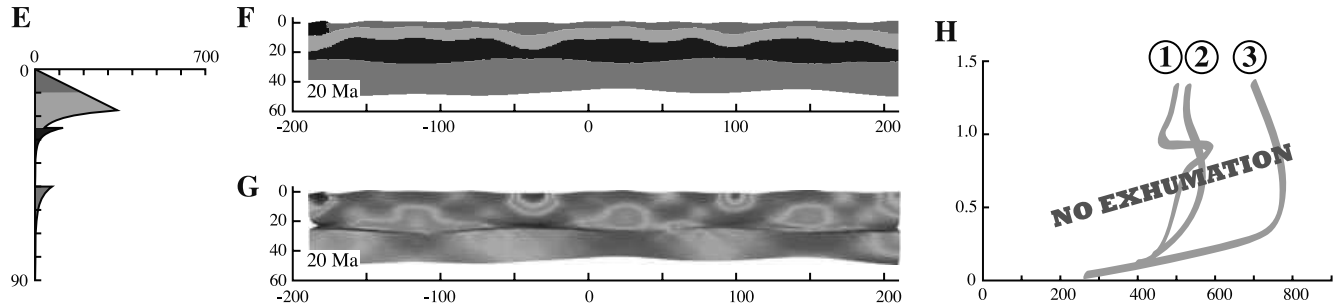
In this experiment, strain localizes between 2 and 12 Myr in the middle and lower crusts resulting in the formation of a dome, which

exhumes mainly lower crustal material (Figs 3F and 6A). Localization occurs after 2 Myr on two conjugate shear zones (sz1a and sz1b) below the graben gl1 (Figs 3F and 6A). A third shear zone located at the bottom of the lower crust (sz1c) is connected to sz1a. These shear zones root at the Moho. After 7 Myr the dome reaches the surface, resulting in a lateral decoupling of the upper crust in two independent blocks. The dome then grows laterally by spreading on a central symmetric graben located at its centre rather than on its flanks. During the growth of the dome, the Moho rises but the whole crust is never ruptured by the shear zones. At 12 Myr, the faults exhuming the dome are inactive whereas two grabens

Cold case (initial Moho temperature: 685 °C)



Intermediate case (initial Moho temperature: 810 °C)



Warm case (initial Moho temperature: 935 °C)

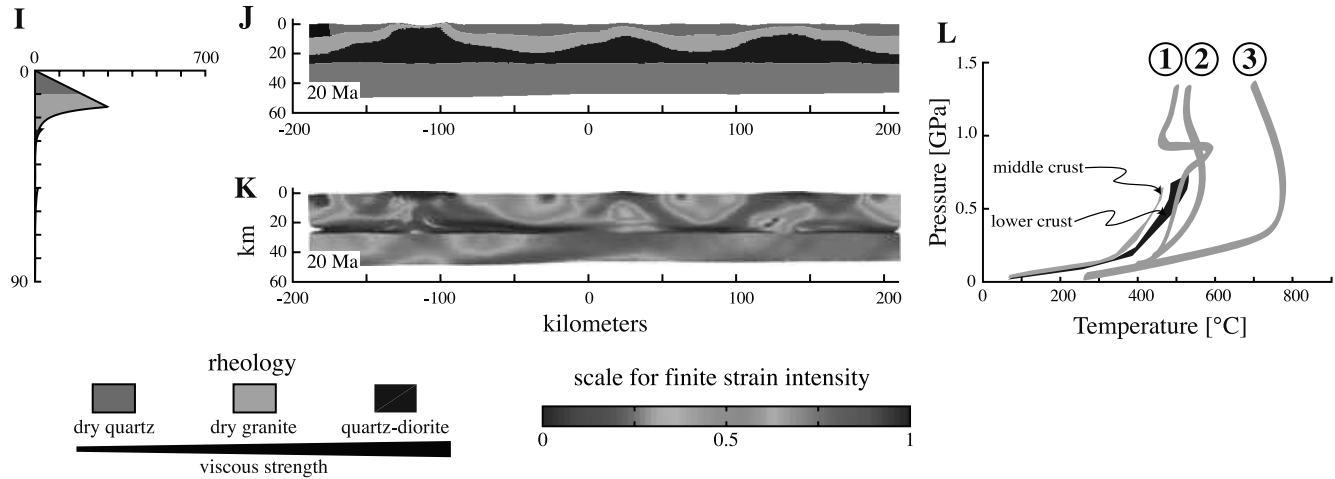


**Figure 4.** Cold, intermediate and warm PS experiments (lithological stratification with more mafic material at depth). Initial strength profiles (A, E and I), geometry (B, F and J) and intensity of finite strain (C, G and K) at the end of the experiment and comparison between the envelopes of the synthetic  $P$ - $T$  paths and the  $P$ - $T$  paths of Tinos (1) (Parra *et al.* 2002) and Naxos (2 and 3) (Martin 2004) (D, H and L). The black portion of the upper crust in (B, F and J) corresponds to a zone of 30 MPa cohesion introduced to avoid localization at the edge of the model. In the cold case, no middle and lower crust is exhumed at the surface; strength localizes in the mantle leading to the formation of a ‘true rift’. In the intermediate cases, no middle and lower crust is exhumed at the surface, homogeneous stretching leads to the formation of a ‘wide rift’. In the warm case, some middle and lower crust is exhumed to the surface in a structure that shares characteristic of the ‘spreading dome’ and the ‘wide rift’ modes. See text for detailed description.

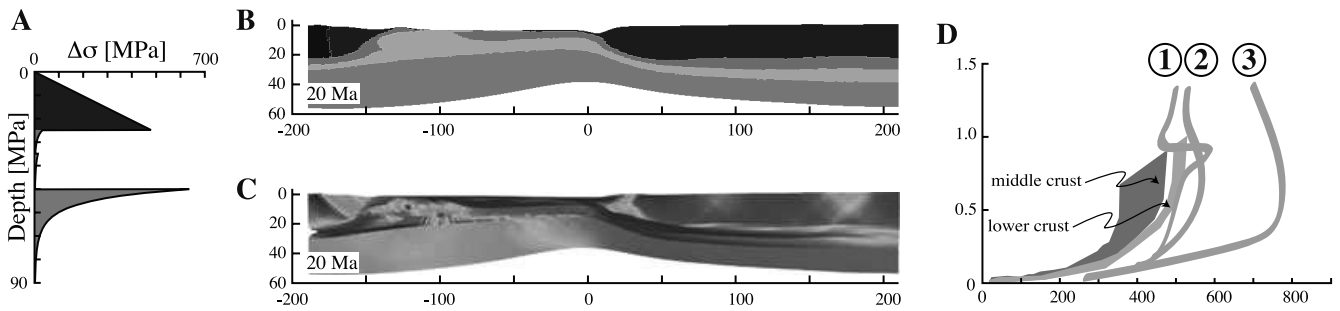
(g2 and g3) are still active. A second dome then forms below graben g2. Its evolution and timing are similar to graben g1: formation of three shear zones in the middle and lower crusts at 14 Myr (sz2a, sz2b and sz2c), exhumation to the surface at 19 Myr and bending of the Moho. During the activity of the second dome (14–19 Myr), the deep parts of the shear zones sz1b and sz1c are still active. sz1b is connected to a newly formed graben at the vicinity of the right flank of the first dome. In the meantime a dome forms below graben g3. It is associated to diffuse conjugate shear zones and does not

pierce the surface. During the last Myr, localized strain only occurs at the Moho.

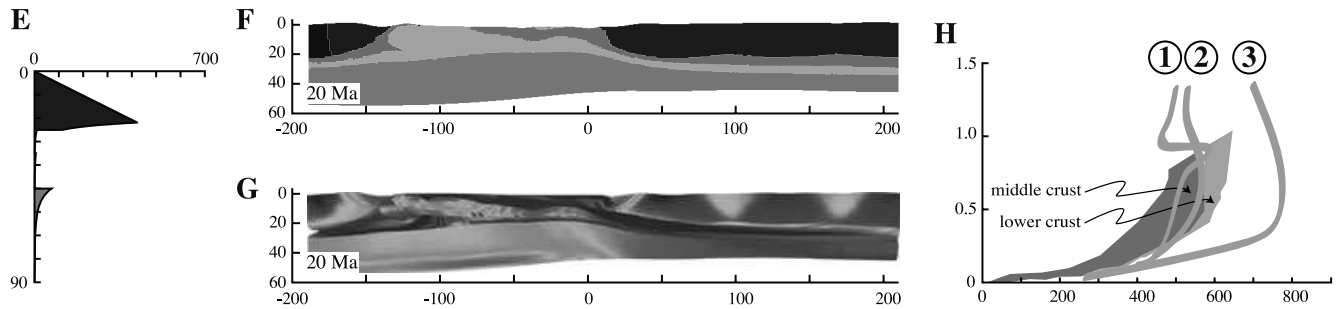
#### 4.2 The ‘pure-shear’ (PS) experiment

Between 2 and 8 Myr, strain localizes in the lower crust resulting in the formation of three lower crustal domes (Figs 4F and 6B). At 3 Myr, three sets of conjugate shear zones (sz1a-b-c, sz2a-b and sz3a) form in the middle and lower crusts below the three grabens

Cold case (initial Moho temperature: 685 °C)



Intermediate case (initial Moho temperature: 810 °C)



Warm case (initial Moho temperature: 935 °C)

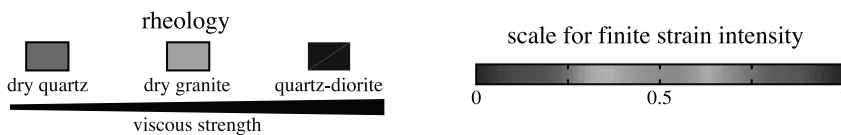
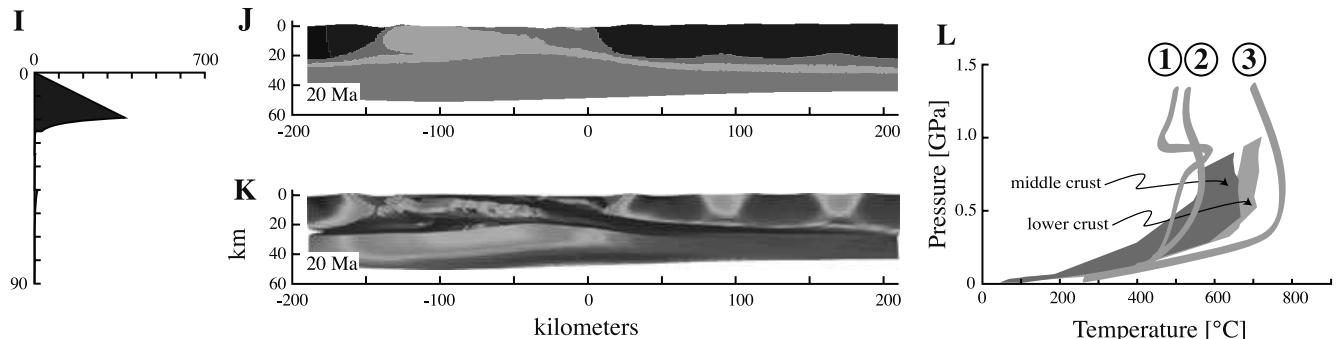


**Figure 5.** Cold, intermediate and warm NS experiments (reversed lithological stratification due to nappe stacking). Initial strength profiles (A, E and I), geometry (B, F and J) and intensity of finite strain (C, G and K) at the end of the experiment and comparison between the envelopes of the synthetic  $P$ - $T$  paths and the  $P$ - $T$  paths of Tinos (1) (Parra *et al.* 2002) and Naxos (2 and 3) (Martin 2004) (D, H and L). The black portion of the upper crust in (B, F and J) corresponds to a zone of 30 MPa cohesion introduced to avoid localization at the edge of the model. In the cold, intermediate and warm cases, middle and lower crust is exhumed at the surface in ‘metamorphic core complex’ mode. See text for detailed description.

(g1–3). At 8 Myr, the lower crust reaches 12–14 km and the three grabens overlying the dome become inactive. Deformation in the upper crust is then localized on three pairs of grabens at both sides of the domes (g1a-b, g2a-b and g3a-b). Each secondary graben is extended at depth by one previously formed shear zone rooting in the middle-lower crust interface. These asymmetric systems allow for the exhumation of lateral subdomes. The final geometry consists in three large domes composed of three subdomes (Fig. 4F). The rise of the top of the lower crust is stopped at 10–12 km. During the last 4 Myr, shear zones develop at the Moho and progressively propagate in the mantle. The resulting geometry is similar to periodically

spaced Cantilever systems (Kuznir & Park 1987). However, the amount of extension in the last 4 Myr is not sufficient to rupture the crust and the mantle.

#### 4.3 The ‘nappe-stacking’ (NS) experiment

In this experiment, grabens g2 and g3 are abandoned at 3 Myr, after initial necking. Strain localization below graben g1 leads to the exhumation of one large dome (Figs 5F and 6C). Between 3 and 5 Myr, two flat lying shear zones extending the upper crustal faults (f1a and f1b) localize in the upper part of the middle crust

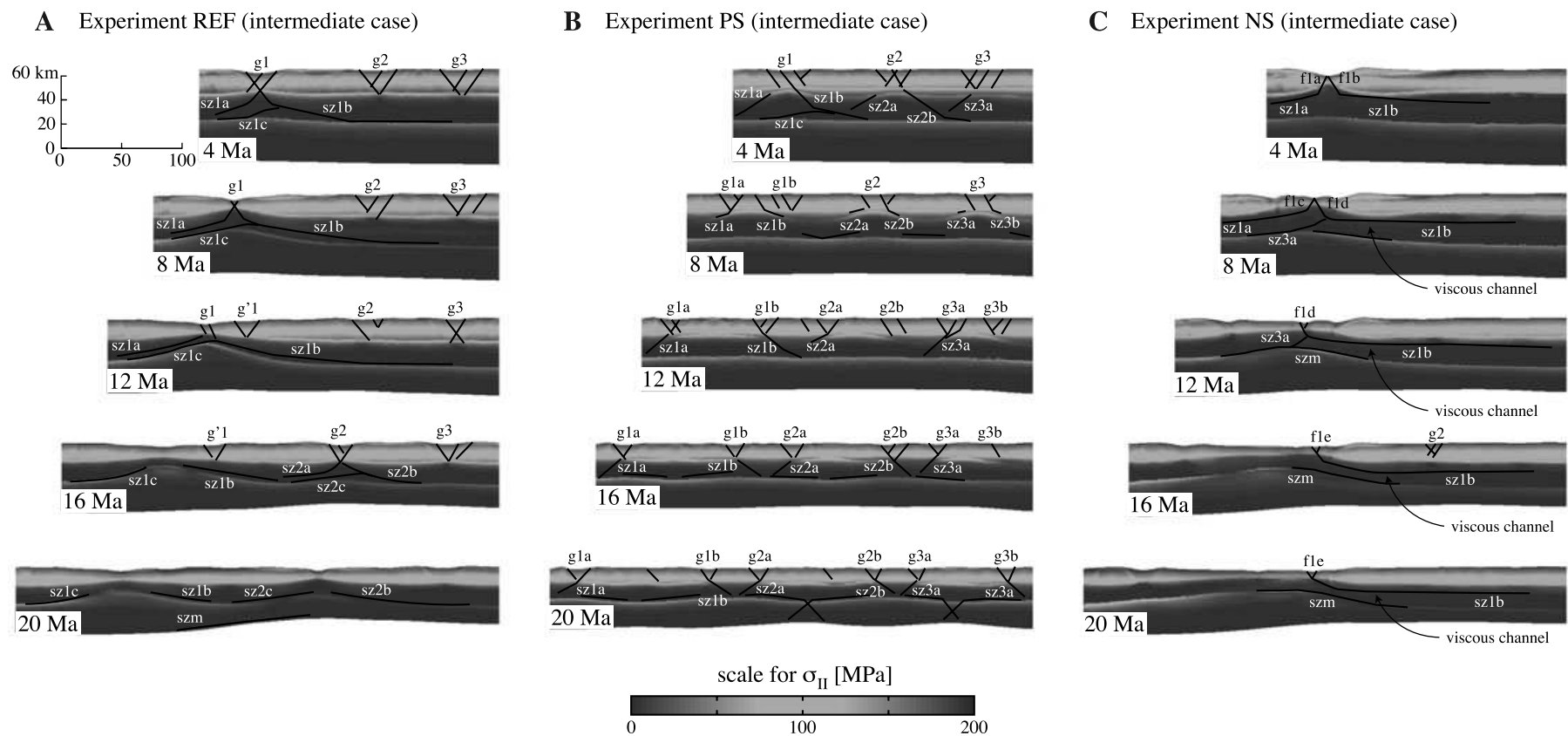


**Figure 6.** Sequential evolution of the intermediate case of experiments REF (A), PS (B) and NS (C). The profiles of second invariant of deviatoric stress indicate the effective shear stress. The zones of localized strain (g: graben, f: faults and sz: shear zones) are reported from strain-rate profiles. See text for detailed description.

(respectively, sz1a and sz1b). This conjugate system allows the vertical ascent of middle-lower crustal material in a dome. The exhumed material pierces the upper crust at 5 Myr. From that stage, the upper crust does not deform any longer. After 6 Myr, the active conjugate faults switch to the centre of the dome (flc and fld). They root in shear zones sz1a and sz1b. Two other shear zones form at the Moho (sz1c and szm). Symmetric lateral growth of the dome occurs during 2 Myr. From 10 to 12 Myr, the left dipping fault (flc) and shear zone (sz1a) progressively inactivate and the dome becomes asymmetric. After 16 Myr, active deformation at the surface switches to the right flank of the dome (fle). The asymmetric lateral growth of the dome is provided by lateral flow of the middle and lower crusts in a viscous channel delimited by two parallel shear zones (sz1b and szm). During this experiment, the exhumation of middle and lower crusts is accompanied by rise of the Moho below the dome. However, no localized strain disrupts the mantle lithosphere.

#### 4.4 Influence of initial thermal profile

For a given lithological stratification, the geometry of the crustal structures accommodating extension is roughly similar, independently of the initial thermal profile. The initial thermal profile has a major influence on the dynamics and the localization of strain in experiments REF and PS. First, the grabens are simultaneously active in the cold cases whereas the grabens activity alternates sequentially in the warm cases. Second, as high temperature profiles favour localization, they also promote exhumation of middle and lower crusts in the grabens. Third, strain localization in the upper crust is only transmitted down to the mantle in the cold cases. These three points explain the discrepancies observed in the final geometry and the finite strain pattern (Figs 3 and 4). On the contrary, the effect of the initial thermal profile is reduced in NS experiments (Fig. 5). Indeed, the final geometry and finite strain pattern of the three NS experiments share the major characteristics described in Section 4.3. Finally, for the three lithological stratifications, the amplitude of the Moho deflection is higher when the initial low initial thermal gradients are low.

## 5 INTERPRETATION OF THE MODELLING RESULTS

In this section, we interpret different stages of our experiments and propose a classification of post-orogenic extensional structures.

### 5.1 Necking of upper crust and downward propagation of localized strain

Strain localization in the regularly spaced grabens during the first 2 Myr can be interpreted as upper crustal plastic necking over the low viscosity lower crust. The 70 km length scale appearing in all experiments is not imposed by any heterogeneity but corresponds to the preferred amplification wavelength of the system. The ratio between the neck spacing and the thickness of the plastic layer hence varies between 2.8 and 4.7, which is in agreement with analytical solutions (3–4) for a non-Newtonian viscous layer overlain by a plastic layer (Fletcher & Hallett 1983).

After this initial event, sets of conjugate shear zones (a and b on Fig. 6) extend the conjugate necking-related faults into the lower viscosity layers. In REF and PS experiments they root at the Moho with a dip decreasing from 60° to 0°, whereas in NS experiments

they root at the low viscosity mid-crustal layer. The downward propagation of the localized shear zones in the middle and lower crusts therefore results from the high strain rates at the lower tip of the faults in association with the non-linear viscous rheology (Burov & Poliakov 2001; Wijns *et al.* 2005). These shear zones accommodate most of the exhumation of the middle and lower crust (Figs 3 and 4).

### 5.2 Dynamics of exhumation

Exhumation of a dome up to the surface occurs in six experiments: intermediate and warm case with the REF stratification, warm case with the PS stratification, and cold, intermediate and warm case with the NS stratification (Figs 3–5). It is therefore favoured by the strength contrast between the upper crust and the middle-lower crust. It is the result of the extreme thinning of the upper crust. The topographic gradient induced by the formation of the necks allows the lateral flow in the middle and lower crusts (Block & Royden 1990), which in turn brings material filling the available space in the neck. Two dynamics are responsible for the exhumation and the lateral growth of the domes. In REF (intermediate and warm) and PS (warm) experiments, most of the exhumation is achieved through a spreading system consisting in conjugate normal faults and shear zones located at the centre of the dome (Fig. 6B). The shear zones rooting in the Moho prevent the formation of a large viscous channel in the middle-lower crust. As a result, most of the domes are formed from lower crustal material. Besides, these domes do not correspond to MCC *stricto sensu*. Since the faults and the shear zones are located at the centre of the dome, they cannot be considered as detachments. In the following, we call these structures spreading domes.

In NS experiments, exhumation occurs in two stages. The first stage is controlled by the vertical ascent of the middle and lower crusts below the graben (Fig. 7D). Exhumation is allowed by two symmetric high angle faults and is maintained by the low viscosity of the lower crustal layers. The rise of the ductile crust is responsible for the flexure of the upper crust illustrated by the strength profile at 4 Myr (Fig. 6C). The second stage is controlled by asymmetric lateral flow in the middle and lower crusts. A steady viscous channel develops between the bottom of the upper crust and the Moho and brings material finally exhumed below the normal faults. The resulting structures can be interpreted as MCC with successive detachments located at the flanks of the dome. Even though the dynamics of exhumation is different in MCC and in spreading domes, the *P-T* paths of the exhumed units show a first-order similarity (Figs 3–5). Cooling is almost inexistent in the first stages of the exhumation. The end of the exhumation is then associated to cooling along warm thermal gradients.

### 5.3 Lateral migration versus strain localization

The degree of localization in a necking zone and the migration of active exhumation from a graben to another are strongly controlled by the strength of the exhumed material, which is controlled by its lithology and its temperature. In REF cases, the exhumed material has the same lithology as the upper crust. The local reduction of crustal strength in the necks is only due to the exhumation of warm material (Fig. 6A). As the exhumed material cools down near the surface, its strength increases. It then becomes easier to rupture the crust at the location of another neck. In PS cases, the three necks are active simultaneously in the first part of the experiments, and

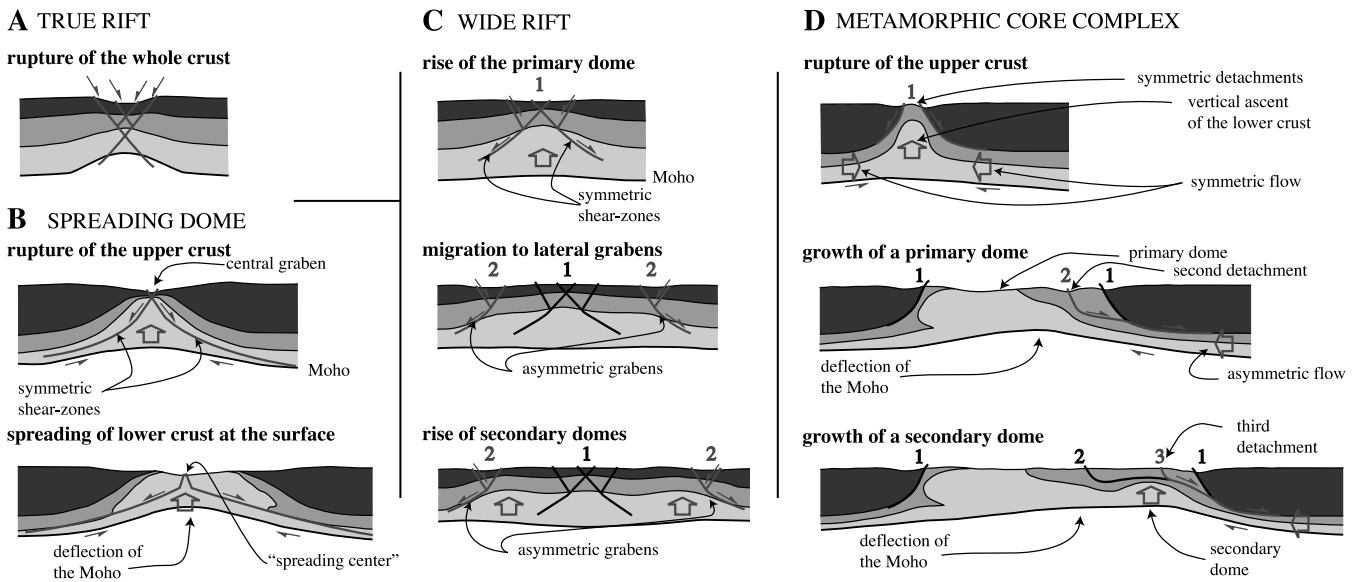


**Figure 7.** Models of evolution for ‘true rift’ mode (A), ‘spreading dome’ mode (B), ‘wide rift’ mode (C) and ‘metamorphic core complex’ mode (D). The evolution of one neck is represented. The active structures are coloured in red. (A) In the ‘true rift’ mode, localized strain is transmitted from an upper crustal graben down to the mantle, leading to the rupture of the whole crust. In this mode, exhumation of the lower crust up to the surface does not occur. (B) In the ‘spreading dome’ mode, the faults are extended by ductile shear zones rooting at the Moho. The symmetric lower crustal dome is exhumed in a ‘spreading centre’ located in the centre of the dome. The Moho is passively deflected below the dome, but it is not ruptured by the shear zones. (C) In the ‘wide rift’ mode, several crustal grabens are simultaneously active (not represented). Lower crust is exhumed below the grabens, but the upper crust is never ruptured and the lower crust never reaches the surface. The rise of high strength material induces the migration of active deformation on newly formed grabens. (D) In the ‘metamorphic core complex’ mode, the lower crust is first exhumed locally. Lateral growth of the dome is then achieved through asymmetric flow of the lower crust. The viscous channel is bounded on top by the detachments, and at bottom by the Moho. Successive detachments allow for the development of secondary domes in the metamorphic core complex.

then extension migrates on pairs of newly formed grabens (Fig. 6C). In these cases, migration is imposed by the slow rise of the high strength lower crust (Fig. 6B). This mode of extension corresponds to the wide rift mode of Buck’s classification (Buck 1991). In NS cases, one neck accommodates all the extension with little migration of the faults. Exhumation of very low strength material prevents deformation to migrate to another neck (Fig. 6C). The initial thermal gradient has an influence on the degree of lateral strain localization in REF and PS experiments, as well. When warm material is exhumed, it induces a reduction of the upper crustal strength. As a consequence, the necks are active for a longer duration in the warm cases, compared to the intermediate cases.

To compare our results with other studies, typical values for the integrated strength of the lithosphere (Ranalli 1995) have a magnitude comprised between  $10^{11}$  N m<sup>-1</sup> (within the grabens) and  $10^{12}$  N m<sup>-1</sup> (within the surrounding parts). Migration of the active deformation and the development of a wide rift are controlled by local increase of the integrated strength, as previously proposed (England 1983; van Wijk & Cloetingh 2002).

#### 5.4 Classification of post-orogenic extensional structures

The results of our experiments suggest that the crustal lithological stratification and the initial temperature profile have a major influence on the dynamics of extension. Four modes of extension have been described here: true rift, spreading dome metamorphic, wide rift and core complex modes (Fig. 7). The last two modes correspond to the classification of Buck (Buck 1991). The true rift mode is characterized by migration of the deformation from the crust down to the mantle. It eventually leads to the rupture of the whole lithosphere that could represent the first step to oceanization.

In this mode, exhumation of ductile crust up to the surface does not occur. The spreading dome mode is characterized by the exhumation of a lower crustal dome along a ‘spreading centre’ located in the centre of the dome. The parallel with oceanic spreading centres is only based on morphology. The wide rift mode is characterized by the simultaneous formation of several crustal necks. However, the upper crust is not ruptured and ductile crust is not exhumed. The metamorphic core complex mode is characterized by extreme strain localization in the upper crust. It is associated with the exhumation of a lower crustal dome below successive detachments located at the edge of the dome.

We propose that the four modes can be classified as a function of the initial Moho temperature and of the ratio of the upper and lower crustal strengths (Table 3). Strength ratios larger than one correspond to metamorphic core complex mode, whatever the initial Moho temperature. For initial Moho temperature lower than 700 °C and for strength ratios larger than or equal to one, true rifts are expected. Wide rift mode is predicted for initial Moho temperature close to 800 °C and for strength ratios lower than one. Spreading dome mode occurs for initial Moho temperature greater than 800 °C and for strength ratios equal to one. Finally, an intermediate mode between wide rift and spreading dome is expected for initial Moho temperature greater than 900 °C and for strength ratio lower than one.

## 6 COMPARISON WITH THE AEGEAN DOMAIN

The initial thermal profile and lithological stratification of the intermediate case of NS experiment has been designed with constraints from the Aegean domain. To compare the results of the experiment

**Table 3.** Different modes of extension of the crust depending on the thermal gradient and the strength ratio between the upper and lower crust computed at the same temperature. If the crust is homogeneous, this ratio equals one (REF experiments). If the lower crust is more mafic than the upper crust, the ratio is lower than one (PS experiments). If the lower crust is less mafic than the upper crust, the ratio is larger than one (NS experiments).

		Strength ratio between the upper and lower crust		
		$R < 1$	$R = 1$	$R > 1$
Initial Moho temperature	$< 700^\circ\text{C}$	True-rift	True-rift	MCC
	$\sim 800^\circ\text{C}$	Wide rift	Spreading dome	MCC
	$> 900^\circ\text{C}$	Spreading dome-wide rift	Spreading dome	MCC

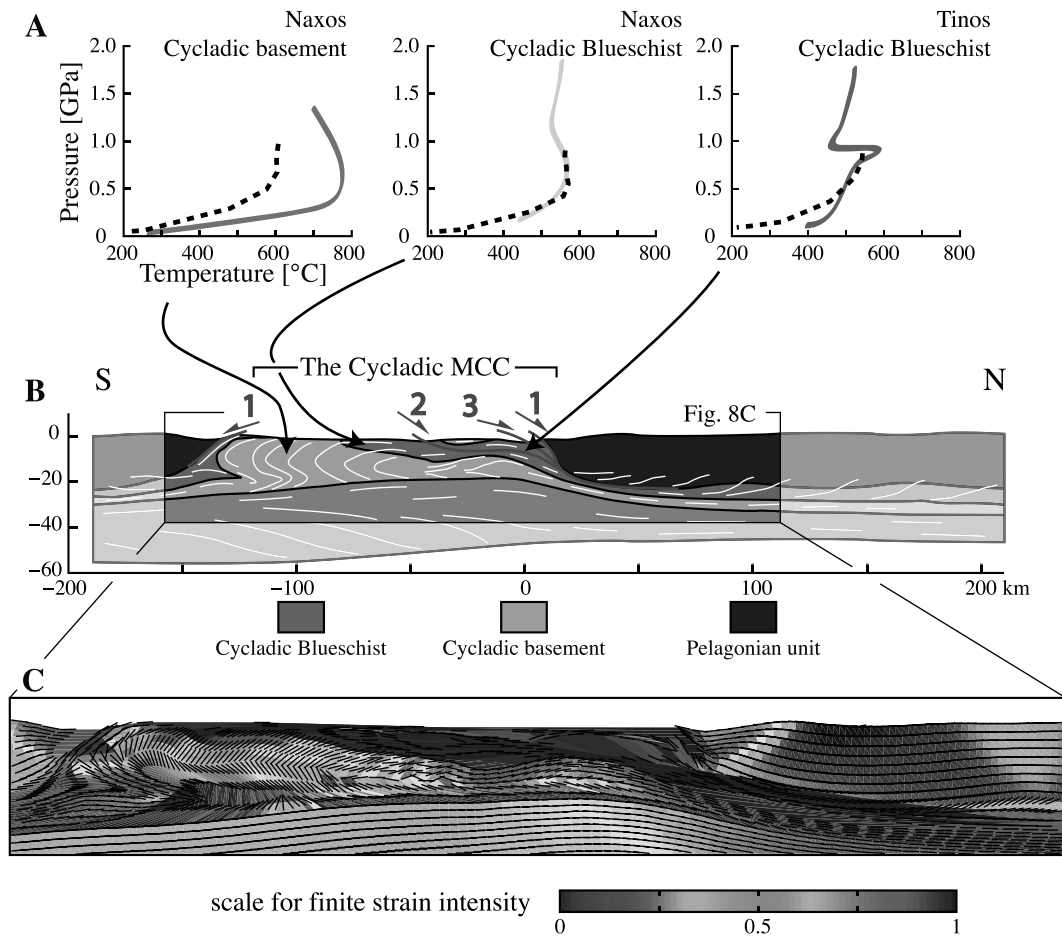


**Figure 8.** Comparison between the intermediate NS model and the Cyclades. (A) Comparison between the synthetic  $P$ - $T$  paths and the natural ones. (B) Geometry and interpolated schistosity at 20 Ma. The three successive detachments are printed in red. (C) Profile of intensity of finite strain and dip of the schistosity (black lines). The intensity of finite strain is represented as  $I = 1 - X/Z$  so that  $I = 1$  means infinite stretching. See comments in text.

to the observations, we consider the final stage as a synthetic N-S cross-section of the Cyclades with the North at the right side of the model (Fig. 8). This 2-D approach cannot account for E-W tectonics in the Cyclades. Syn-extensional E-W shortening has indeed been documented in the MCC (Avigad *et al.* 2001), although its effect has been argued to be limited (Gautier & Brun 1994). The Cyclades are also characterized by a gradient of finite extension along strike from its periphery in continental Greece to its centre around Naxos island. The synthetic profile cannot be directly compared to the present day geometry of the Cyclades, which is affected by steep normal faults that dissect the structures associated to the MCC formation. Moreover, the MCC correspond to topographical low in our experiments whereas they correspond to topographical

high in the Cyclades (most probably due to our choice of density in the crust *cf.* Section 7.1).

### 6.1 Crustal geometry

The distribution of domes and units predicted by the experiments matches the Cyclades one (Figs 1A and 8B). In both nature and experiments, the Cycladic basement is located in the southern and central part of the profile. We propose that the large dome cored by the basement in the centre of model is equivalent to the central MCC of Naxos and Paros, and that the secondary dome corresponds to the northern MCC of Andros, Tinos, Mykonos and Ikaria. According to this interpretation, the Cyclades would correspond to one large

MCC comprising several subdomes exhumed below distinct detachments. Tinos and Naxos, which are well-documented islands, are therefore considered as representative of the northern and central MCC, respectively. In the experiment, the final crustal thickness below the MCC is comprised between 18 and 27 km (Fig. 8B), whereas in the Cyclades, the crust is 25 km thick (Tirel *et al.* 2004b). Furthermore, the present-day Moho is flat in the Cyclades and does not exhibit the vertical deflection obtained in our experiment. This deflection is the result of the contribution of the low viscosity lithospheric mantle to the isostatic compensation (Wijns *et al.* 2005). It is possible that the flat Moho geometry in the Cyclades is not inherited from the MCC formation event, but represents a later feature. The active MCC in the D'Entrecasteaux islands show a Moho upwarp of 10–15 km (Abers *et al.* 2002). Modelling of gravity data in the D'Entrecasteaux islands shows that crustal thinning alone leads to subsidence. This implies that deep mantle takes part in MCC topographic signature. Our experiment, considering a 90-km-thick lithosphere without underlying asthenosphere and lasting for relatively short time cannot render possible late flattening of the Moho.

## 6.2 Finite deformation and kinematics

The finite deformation intensity (Fig. 8C) indicates that finite strain is partitioned between the little deformed Pelagonian upper unit, the highly sheared Cycladic Blueschist and the less deformed basement unit. Maximum finite deformation intensity occurs at the rheological boundaries (Fig. 8C), mainly at the top of the Cycladic Blueschist that represent the sharpest strength contrast as observed in the Cyclades (Mehl *et al.* 2005). The computed schistosity is fairly flat at the surface. In the deep basement, the steep schistosity is the result of the ascent of the lower crust following necking. This pattern is consistent with the schistosity trajectories within and around the core of Naxos dome, which was interpreted as an evidence for diapiric ascent (Vanderhaeghe 2004). Besides, the dip and the kinematics of the detachments (Fig. 8B) reflect the dominant top-to-the-north sense of shear in the Cycladic MCC. The deformation associated with the initial conjugate south-dipping detachment does not have known analogues in nature. The top-to-the-south shear criteria documented on Ios island are indeed linked to thrusting of the Cycladic Blueschist over the Cycladic basement (Huet *et al.* 2009) and the top-to-the-south criteria described in the western Cyclades correspond to late Miocene extension (Iglseider *et al.* 2009).

## 6.3 *P-T* paths

The distribution of the synthetic *P-T* paths (Fig. 8A) shows that cooling occurs early during decompression on the northern flank of the dome (equivalent to Tinos) and that cooling happens later in the core of the dome (equivalent to Naxos). This zonation observed in the Cyclades has been interpreted by the effect of small-scale heat conduction between the upper and the lower units (Jolivet & Goffé 2000). The synthetic *P-T* paths of the Cycladic Blueschist (Tinos and Naxos) are in good agreement with their natural equivalent (Parra *et al.* 2002; Martin 2004, Fig. 8A). Such a fit cannot be observed with the other experiments (Figs 3–5). However, the experiment is not able to reproduce the *P-T* path (Fig 8A) of the migmatitic core of Naxos that reached 800 °C (Martin 2004). Two processes could have lead to a better fit. First, account for partial melting would lead to a decrease of the effective viscosity and density of a part of the material (e.g. Rey *et al.* 2009), and could

probably promote the exhumation of the lowest part of the crust. Second, concentration of radiogenic elements in migmatites, that is not considered in our experiments, is likely to explain the observed retrograde heating (Thomson & Bard 1982).

## 7 DISCUSSION

In this section, we discuss the mechanical feasibility of cold MCC and the need for strength discontinuity at the BDT for the initiation of MCC.

### 7.1 The effect of density contrast and radiogenic heating

Among parameters neglected in the experiments, radiogenic heating could probably affect thermal state during extension, while density contrast between the upper and lower crust could control the overall geometry and exhumation rates. Test experiments with radioactive heating term ( $H_r$ , eq. 2) in the granitic lower crust were performed and showed no important effect of this parameter on the geometry of isotherms or *P-T* paths shapes. The 20 Myr time spans considered here are probably too short and exhumation rates too high for radioactive decay to affect the thermal evolution of exhumed rocks. Furthermore, the simple initial thermal conditions used for our experiments do not consider any thermal effect of the nappe-stacking event on geotherm, that would result in colder initial profiles.

The effect of density contrast between the upper and lower crust has been estimated for the REF and NS geometries with density contrast values ranging from 0 to 300 kg m<sup>-3</sup> (Fig 9A). The experiments show that the overall geometries are not changed except the surface topography, that is negative throughout the dome for  $\Delta\rho = 0$  and reached +2000 m for  $\Delta\rho = 300$  kg m<sup>-3</sup>. To evaluate the possible participation of density contrasts in exhumation processes (i.e. diapirism), maximum exhumation rates have been compared to exhumation rates calculated for equivalent markers exhumed by pure shear thinning (Fig 9B). It appears that exhumation rates are controlled by the extension rate imposed at the boundary and that density contrast only has a second-order effect. Diapirism is therefore not directly involved in the MCC modelled here.

### 7.2 MCC are not restricted to warm lithospheres

Our results confirm that the mode of extension in thickened crusts is primarily controlled by rheological stratification (Brun 1999; Wijns *et al.* 2005). Strong competence contrasts between the upper and lower crusts ensure efficient flow of the lower crust and localized stretching of the upper crust. They therefore promote the formation of MCC. However, whereas the rheological stratification is classically controlled by temperature, it is controlled at first order by the lithological stratification in our experiments. This approach gives new insights on the ability of MCC to form in a relatively cold crust. In numerical experiments where the crustal lithology is homogeneous, MCC are predicted to form for initial Moho temperature higher than 800 °C (Tirel *et al.* 2008) with effective viscosities lower than 10<sup>20</sup> Pa s for the lower crust and 10<sup>22</sup> Pa s for the mantle. A MCC forms in our three NS experiments, even for initial Moho temperature slightly lower than 700 °C. In these cases, the lithological stratification ensures effective viscosities in the range proposed by (Tirel *et al.* 2008). We therefore suggest that MCC can form in relatively cold crust, provided the lithology of the lower crust ensures sufficiently low viscosity.

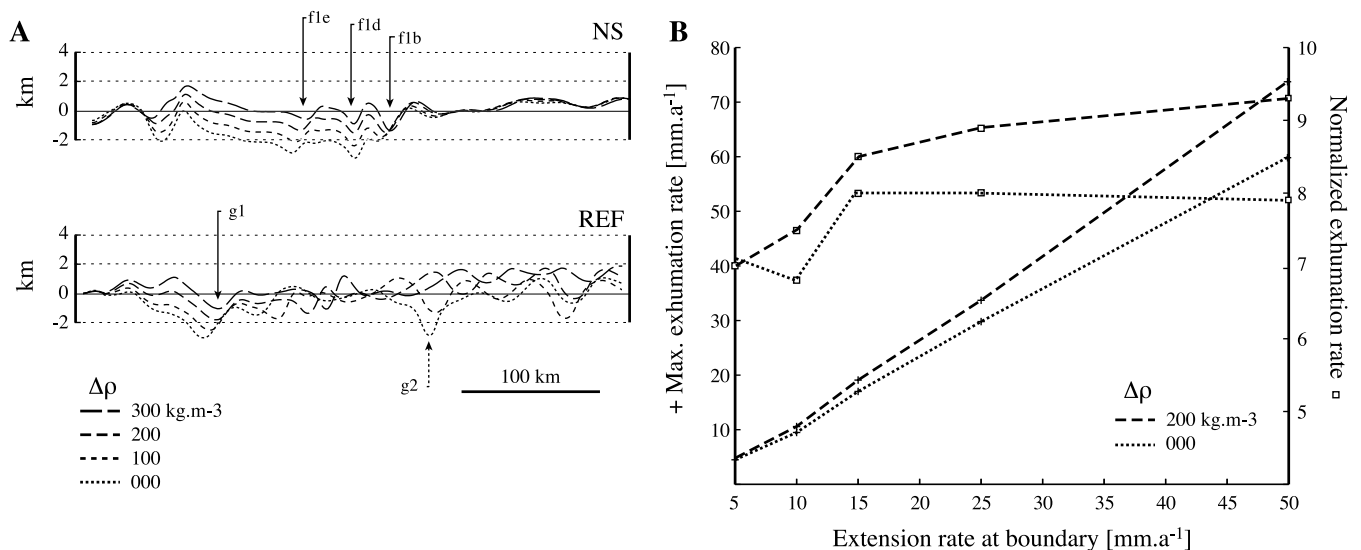


**Figure 9.** Effect of density contrast on topography and exhumation rates. (A) Topography profiles for the NS and REF intermediate cases with density contrast ( $\Delta\rho$ ) between the upper and lower crust. Lower crust is lighter than the upper crust. flb, fld and fle refer to faults that develop in NS experiments, g1 and g2 refer to grabens forming in REF experiments (see Fig. 7 for detailed geometry of strain localization). (B) Maximum exhumation rate versus extension rate imposed at boundary in the NS experiment. Normalized exhumation rates are maximum exhumation rates divided by the theoretical exhumation rate of markers at the same initial depth and exhumed only by pure shear thinning of the material. Density contrast (positive for lower crust lighter than upper crust) has only a second-order effect on exhumation rate values.

Two processes associated to nappe stacking can produce this pattern. First, obduction consist of thrusting of strong ophiolitic material over weaker continental crust. Second, it has been argued that the mafic lower crust delaminates in the formation of mountain belts (Laubscher 1990). The combination of these two processes is thus likely to lead to the formation of a reverse rheological stratification, favouring in turn the formation of cold MCC. In this point of view, the setup of laboratory experiments with thickened crusts (Brun *et al.* 1994; Tirel *et al.* 2006) can be reinterpreted. The rheological stratification is reproduced by modelling the upper crust with a Mohr-Coulomb plastic material (sand) and the lower crust with a Newtonian viscous material (silicone). The lower layer has a constant low viscosity, which is an approximation of the thermally controlled viscous lower crust. However, the resulting strength profiles are similar to those of our NS experiments. We therefore propose that the rheological stratification of laboratory experiments corresponds to a lithological stratification that could be the result of nappe stacking.

Besides, the dynamics and final geometry of NS experiments is hardly affected by the initial thermal profile, even if the initial strength profiles strongly differ (Fig 5). In the cold case, an important part of the lithospheric strength resides in the lithospheric mantle (Fig 5A), as in the ‘jelly sandwich’ model (Burov & Watts 2006), whereas, in the warm case, the whole strength of the lithosphere resides in the crust (Fig 5I), as in the ‘crème brûlée’ model (Jackson 2002). As a consequence, whether the mantle is strong or not does not influence the formation of MCC in NS experiments. The low viscosity lower crust is responsible for efficient decoupling between the upper crust and the mantle and prevents downward propagation of localized strain to the lithospheric mantle. We therefore suggest that the development of MCC is not sufficient to discriminate the long-term behaviour of the lithosphere, especially in the Aegean. The propagation of the North Anatolian fault in the Aegean lithosphere (Armijo *et al.* 1999) is for instance not in contradiction with the development of MCC in the same lithosphere.

### 7.3 High temperature alone is not sufficient for the development of MCC

In the intermediate and warm cases of experiments REF, the initial Moho temperature is higher than 800 °C. MCC formation is then predicted in this range (Tirel *et al.* 2008). However, extension is accommodated in spreading dome mode in our experiments. Besides, in numerical studies considering homogeneous crust similar to our REF experiments, two types of structures are obtained, both of them being interpreted as MCC. When no localizing heterogeneity is considered, several domes develop in upper crustal necks and shear zones are located at their centres (Wijns *et al.* 2005; Tirel *et al.* 2009). This dynamics is similar to the spreading dome mode according to our classification. On the contrary, when a localizing heterogeneity is introduced, only one dome is exhumed below a detachment located on its flanks (Tirel *et al.* 2004a; Tirel *et al.* 2008). These structures correspond to MCC *stricto sensu*. The pre-scripted heterogeneity has therefore a major effect on the dynamics of extension and exhumation. First, it localizes strain in a unique neck. Second, the detachment develops within the heterogeneity. We then suggest that the presence of a localizing heterogeneity, responsible for strength discontinuity at the top of the lower crust, is essential for the formation of MCC since it prevents the formation of shear zones dissecting the whole lower crust, as in spreading domes. In experiments NS, the weak middle crust has an effect similar to the heterogeneity in previous numerical models (Tirel *et al.* 2004a; Tirel *et al.* 2008). It is responsible for a major strength drop at the BDT (Fig 5), precisely where the crustal strength is supposed to be the largest (Brace & Kohlstedt 1980). The middle crustal layer acts then like a décollement just below the BDT, allowing the localization of detachments. This dynamics can be compared to the effect of reaction softening assisted by surface fluids stopped at the BDT (Famin *et al.* 2004). Retrograde mineral reactions developing in a few thousands of years are able to produce a large strength drop at the BDT (Gueydan *et al.* 2004). These processes are likely to

explain the development of normal shear zones at the BDT within a homogeneous crust submitted to extension.

## 8 CONCLUSION

The aim of this paper is to explore the influence of lithological stratification inherited from orogenic stages on the development of MCC during post-orogenic extension. Three crustal stratifications (homogeneous, normal and reversed) and three thermal profiles (cold, intermediate and warm) have been considered. In the nine numerical experiments, the degree of strain localization and the dynamics of exhumation are strongly controlled by the crustal stratification, and, to a lesser extent, by the temperature profile. Four modes of extension have been distinguished: true rift, wide rift, metamorphic core complex and spreading dome. Spreading dome accommodates stretching by the exhumation of material along a ridge located in the centre of the dome.

A metamorphic core complex can develop in a crust where the lithological layering is reversed, even with cold thermal gradients. In a homogeneous crust or a normally stratified crust, no metamorphic core complex forms, even with high thermal gradients. High thermal gradients are therefore neither sufficient nor necessary for the development of MCC in thickened crusts submitted to post-orogenic extension. The lithological layering and the thermal profile of one of our experiments have been designed with data from the Cycladic MCC. The comparison between the natural data (geometry, finite strain, kinematics and *P-T* paths) and their synthetic counterparts shows a good agreement between our model and nature. In experiments showing the development of a metamorphic core complex, the mantle strength has little influence on the dynamics of exhumation and the final geometry. The presence of MCC is therefore not sufficient to discriminate between the ‘jelly-sandwich’ and ‘crème-brûlée’ long-term strength models.

## ACKNOWLEDGMENTS

This research is a contribution to the ANR-EGEO project. Reviews by two anonymous reviewers helped improving the manuscript.

## REFERENCES

Abers, G.A., Ferris, A., Craig, M., Davies, H., Lerner-Lam, A.L., Mutter, J.C. & Taylor, B., 2002. Mantle compensation of active metamorphic core complexes at Woodlark rift in Papua New Guinea, *Nature*, **418**, 862–865.

Altherr, R., Kreuzer, H., Wendt, I., Lenz, H., Wagner, G.A., Keller, J., Harre, W. & Hohndorf, A., 1982. A late oligocene/early miocene high temperature belt in the attic-cycladic crystalline complex (SE Pelagonian, Greece), *Geologische Jahrb.*, **23**, 97–164.

Armijo, R., Meyer, B., Hubert, A. & Barka, A., 1999. Westward propagation of the north Anatolian into the northern Aegean: timing and kinematics, *Geology*, **27**, 267–270.

Avigad, D., Ziv, A. & Garfunkel, Z., 2001. Ductile and brittle shortening, extension-parallel folds and maintenance of crustal thickness in the central Aegean (Cyclades, Greece), *Tectonics*, **20**, 277–287.

Block, L. & Royden, L., 1990. Core complex geometries and regional scale flow in the lower crust, *Tectonics*, **9**, 557–567.

Bonneau, M., 1984. Correlation of the Hellenic nappes in the south-east Aegean and their tectonic reconstruction, in *The Geological Evolution of the Eastern Mediterranean*, *Geol. Soc. Lond., Spec. Pub.*, **17**, 517–527.

Brace, W.F. & Kohlstedt, D.L., 1980. Limits on lithospheric stress imposed by laboratory experiments, *J. geophys. Res.*, **85**, 6248–6252.

Brun, J.-P., 1999. Narrow rifts versus wide rifts: inferences for the mechanics of rifting from laboratory experiments, *Phil. Trans. R. Soc., Lond.*, **357**, 695–712.

Brun, J.-P., Sokoutis, D. & Van Den Driessche, J., 1994. Analogue modeling of detachment fault systems and core complexes, *Geology*, **22**, 319–322.

Buck, R.W., 1991. Modes of continental lithospheric extension, *J. geophys. Res.*, **96**, 20 161–20 178.

Burov, E. & Poliakov, A., 2001. Erosion and rheology controls on synrift and postrift evolution: verifying old and new ideas using a fully coupled numerical model, *J. geophys. Res.*, **106**, 16 461–16 481.

Burov, E. & Watts, A.B., 2006. The long-term strength of continental lithosphere: “jelly sandwich” or “crème brûlée”? *GSA Today*, **16**, 4–10.

Chéry, J., 2001. Core complex mechanics: from the Gulf of Corinth to the snake range, *Geology*, **29**, 439–442.

Chopra, P.N. & Paterson, M.S., 1984. The role of water in the deformation of dunite, *J. geophys. Res.*, **89**, 7861–7876.

Coney, P.J., 1980. Cordilleran metamorphic core complexes: an overview, *Geol. Soc. Am. Memoirs*, **153**, 7–31.

Cundall, P.A., 1989. Numerical experiments on localization in frictional materials, *Ing. Arch.*, **59**, 148–1598.

England, P., 1983. Constraints on extension of continental lithosphere, *J. geophys. Res.*, **88**, 1145–1152.

Famin, V., Philippot, P., Jolivet, L. & Agard, P., 2004. Evolution of hydrothermal regime along a crustal shear zone, Tinos Island, Greece, *Tectonics*, **23**, doi:10.1029/2003TC001509.

Fletcher, R.C. & Hallet, B., 1983. Unstable extension of the lithosphere: a mechanical model for basin-and-range structure, *J. geophys. Res.*, **88**, 7457–7466.

Gaudemer, Y., Jaupart, C. & Tapponnier, P., 1988. Thermal control on post-orogenic extension in collision belts, *Earth planet. Sci. Lett.*, **89**, 48–62.

Gautier, P. & Brun, J.-P., 1994. Crustal-scale geometry and kinematics of late-orogenic extension in the central Aegean (Cyclades and Ewia Island), *Tectonophysics*, **238**, 399–424.

Gautier, P., Brun, J.-P. & Jolivet, L., 1993. Structure and kinematics of Upper Cenozoic extensional detachment on Naxos and Paros (Cyclades Islands, Greece), *Tectonics*, **12**, 1180–1194.

Gerya, T., Maresch, W.V., Willner, A.P., vanÈReenen, D.D. & Smit, C.A., 2001. Inherent gravitational instability of thickened continental crust regionally developed low- to medium-pressure granulite facies metamorphism, *Earth planet. Sci. Lett.*, **190**, 221–235.

Gueydan, F., Leroy, Y. & Jolivet, L., 2004. Mechanics of low-angle extensional shear zones at the brittle-ductile transition, *J. geophys. Res.*, **109**, doi:10.1029/2003JB002806.

Hansen, F.D. & Carter, N.L., 1982. Creep of Selected Crustal Rocks at 1000 MPa, *EOS, Trans. Am. geophys. Un.*, **63**, 437.

Huet, B., Labrousse, L. & Jolivet, L., 2009. Thrust or detachment? Exhumation processes in the Aegean: insight from a field study in Ios (Cyclades, Greece), *Tectonics*, **28**, doi:10.1029/2008TC002397.

Huisman, R.S., Buitter, S.J.H. & Beaumont, C., 2005. The effect of plastic-viscous layering and strain-softening on mode selection during lithospheric extension, *J. geophys. Res.*, **110**, doi:10.1029/2004JB003114.

Iglseder, C., *et al.* 2009. I and S-type plutonism on Serifos (W-Cyclades, Greece), *Tectonophysics*, **473**, 69–83.

Jackson, J.A., 2002. Strength of the continental lithosphere: time to abandon the jelly sandwich?, *GSA Today*, **2**, 4–10.

Jacobshagen, V., Durr, S., Kockel, F., Kopp, K.O., Kowalczyk, G., Berckheimer, H. & Buttner, D., 1978. Structure and geodynamic evolution of the Aegean region, in *Alps, Apennines, Hellenides report 38*, pp. 537–564, eds Cloos, H., Roeder, D. & Schmidt, K., IUGG, Stuttgart.

Jansen, J.B.H. & Schuilling, R.D., 1976. Metamorphism on Naxos: petrology and geothermal gradients, *Am. J. Sci.*, **276**, 1225–1253.

Jolivet, L. & Brun, J.-P., 2009. Cenozoic geodynamic evolution of the Aegean, *Int. J. Earth Sci.*, **99**, doi:10.1007/s00531-008-0366-4.

Jolivet, L. & Faccenna, C., 2000. Mediterranean extension and the Africa-Eurasia collision, *Tectonics*, **19**, 1095–1106.

Jolivet, L. & GoffŽ, B., 2000. Les dômes métamorphiques extensifs, *Comptes Rendus de l’Academie des Sci.*, **320**, 739–751.

- Jolivet, L., Lecomte, E., Huet, B., Denèle, Y., Lacombe, O., Labrousse, L., Le Pourhiet, L. & Mehl, C., 2010. The North Cycladic detachment system, *Earth planet. Sci. Lett.*, **289**, 87–104.
- Katzir, Y., Matthews, A., Garfunkel, Z., Schliestedt, M. & Avigad, D., 1996. The tectono-metamorphic evolution of a dismembered ophiolite (Tinos, Cyclades, Greece), *Geol. Mag.*, **133**, 237–254.
- Kuznir, N.J. & Park, R.G., 1987. The extensional strength of the continental lithosphere: its dependence on geothermal gradient, and crustal composition and thickness, *Geol. Soc. Lond., Spec. Pub.*, **28**, 35–52.
- Laubscher, H., 1990. The problem of the Moho in the Alps, *Tectonophysics*, **182**, 9–21.
- Lavir, L., Buck, W.R. & Poliakov, A., 1999. Self-consistent rolling-hinge model for the evolution of large-offset low angle normal faults, *Geology*, **27**, 1127–1130.
- Le Pichon, X. & Angelier, J., 1981. The Aegean Sea, *Phil. Trans. R. Soc., Lond.*, **300**, 357–372.
- Le Pourhiet, L., Burov, E. & Moretti, I., 2004. Rifting through a stack of inhomogeneous thrusts (the dipping pie concept), *Tectonics*, **23**, doi:10.1029/2003TC001584.
- Martin, L., 2004. Signification des âges U-Pb sur zircon dans l'histoire métamorphique de Naxos et Ikaria (Cyclades, Grèce), PhD thesis, Université H. Poincaré.
- McKenzie, D.P., 1978. Active tectonics of the Alpine-Himalayan belt: the Aegean Sea and surrounding regions, *J. R. Astron. Soc.*, **55**, 217–254.
- Mehl, C., Jolivet, L. & Lacombe, O., 2005. From ductile to brittle: evolution of localization of deformation below a crustal detachment (Tinos, Cyclades, Greece), *Tectonics*, **24**, TC4017, doi:10.1029/2004TC001767.
- Okrusch, M. & Broecker, M., 1990. Eclogites associated with high-grade blueschists in the Cyclades archipelago, Greece: a review, *Eur. J. Mineral.*, **2**, 451–478.
- Parra, T., Vidal, O. & Agard, P., 2002. A thermodynamic model for FeMg dioctahedral K white micas using data from phase-equilibrium experiments and natural pelitic assemblages, *Contrib. Mineral. Petrol.*, **143**, 706–732.
- Poliakov, A., Podladchikov, Y. & Talbot, C., 1993. Initiation of salt diapirs with frictional overburden: numerical experiments, *Tectonophysics*, **228**, 199–210.
- Ranalli, G., 1995. *Rheology of the Earth*, 2nd edn, Chapman & Hall, London, 413pp.
- Ranalli, G. & Murphy, D.C., 1987. Rheological stratification of the lithosphere, *Tectonophysics*, **132**, 281–295.
- Rey, P., Teyssier, C. & Whitney, D.L., 2009. Extension rates, crustal melting, and core complex dynamics, *Geology*, **37**, 391–394.
- Thomson, P.T. & Bard, J.P., 1982. Isograds and mineral assemblages in the eastern axial zone, Montagne Noire (France): implications for temperature gradients and P-T history, *Can. J. Earth Sci.*, **19**, 129–143.
- Tirel, C., Brun, J.-P. & Burov, E., 2004a. Thermomechanical modelling of extensional gneiss domes, in *Gneiss Domes in Orogeny*, Vol 380, pp. 67–78, eds Whitney, D.L., Teyssier, C. & Siddoway, C.S., Geological Society of America, Boulder, CO.
- Tirel, C., Gueydan, F., Tiberi, C. & Brun, J.-P., 2004b. Aegean crustal thickness inferred from gravity inversion. Geodynamical implications, *Earth planet. Sci. Lett.*, **228**, 267–280.
- Tirel, C., Brun, J.-P. & Sokoutis, D., 2006. Analogue modeling of detachment fault systems and core complexes, *Tectonics*, **25**, doi:10.1029/2005TC001804.
- Tirel, C., Brun, J.-P. & Burov, E., 2008. Dynamics and structural development of metamorphic core complexes, *J. geophys. Res.*, **113**, doi:10.1029/2005JB003694.
- Tirel, C., Gautier, P., van Hinsbergen, D.J. & Wortel, M.J.R., 2009. Sequential development of interfering metamorphic core complexes: numerical experiments and comparison with the Cyclades, Greece, *Geol. Soc. Lond.*, **311**, 257–292.
- Toussaint, G., Burov, E. & Avouac, J.-P., 2004. Tectonic evolution of a continental collision zone: a thermomechanical numerical model, *Tectonics*, **23**, doi:10.1029/2003TC001604.
- Vandenberg, L.C. & Lister, G.S., 1996. Structural analysis of basement tectonics from the Aegean metamorphic core complex of Ios, Cyclades, Greece, *J. Struct. Geol.*, **18**, 1437–1454.
- Vanderhaeghe, O., 2004. Structural record of the Naxos dome formation, in *Gneiss Dome in Orogeny*, Vol 380, pp. 211–227, eds Whitney, D.L., Teyssier, C. & Siddoway, C.S., Geological Society of America Special Paper, Boulder, CO.
- Wdowinski, S. & Axen, G.J., 1992. Isostatic rebound due to tectonic denudation: a viscous flow model of a layered lithosphere, *Tectonics*, **11**, 303–315.
- Wernicke, B., 1990. The fluid crustal layer and its implications for continental dynamics, in *Cross-Sections of the Continental Crust*, pp. 509–544, eds Salisbury, M.H. & Fountain, D.M., Kluwer, Dordrecht.
- Whitney, D.L., Teyssier, C. & Vanderhaeghe, O., 2004. Gneiss domes and crustal flow, in *Gneiss Domes in Orogeny*, Vol. 380, pp. 15–33, eds Whitney, D.L., Teyssier, C. & Siddoway, C.S., Geological Society of America Special Paper, Boulder, CO.
- Wijbrans, J.R. & McDougall, I., 1986. <sup>40</sup>Ar/<sup>39</sup>Ar dating of white micas from an alpine high-pressure metamorphic belt on Naxos (Greece): the resetting of the argon isotopic system, *Contrib. Mineral. Petrol.*, **93**, 187–194.
- van Wijk, J.W. & Cloetingh, S.A.P.L., 2002. Basin migration caused by slow lithospheric extension, *Earth planet. Sci. Lett.*, **198**, 275–288.
- Wijns, C., Weinberg, R., Gessner, K. & Moresi, L., 2005. Mode of crustal extension determined by rheological layering, *Earth planet. Sci. Lett.*, **236**, 120–134.
- Yamato, P., Agard, P., Burov, E., Le Pourhiet, L., Jolivet, L. & Tiberi, C., 2007. Burial and exhumation in a subduction wedge: mutual constraints from thermomechanical modeling and natural P-T-t data (Schistes Lustrés, western Alps), *J. geophys. Res.*, **112**, doi:10.1029/2006JB004441.

## SUPPORTING INFORMATION

Additional Supporting Information may be found in the online version of this article:

**Movies.** Sequential development of the nine experiments presented in the paper. REF, PS, NS refer to reference, initial pure shear thickening and initial nappe stacking. 1100, 1300, 1500 refer to initial bottom temperature.

Please note: Wiley-Blackwell are not responsible for the content or functionality of any supporting materials supplied by the authors. Any queries (other than missing material) should be directed to the corresponding author for the article.